water

MDPI

Article

Mining-Influenced Water from the Abandoned Hausham Colliery in Southern Germany—A Case of Unmonitored Natural Attenuation

Sylke Hilberg [1,*], Nicola Yousefi [1] and Thomas Rinder [1,2]

[1] Department of Environment & biodiversity, University of Salzburg, Hellbrunner Straße 34, 5020 Salzburg, Austria
[2] AFRY Austria GmbH, Strubergasse 30, 5020 Salzburg, Austria
* Correspondence: sylke.hilberg@plus.ac.at; Tel.: +43-662-80445465

Abstract: Coal mining in Upper Bavaria ended in the 1960s and the mines were flooded. This study investigates the mining-influenced water and its environmental implications in the Hausham Mine, one of many unmonitored coal mines in the region and along the northern edge of the Molasse zone in Austria, Germany and Switzerland. Water and solid samples were collected in the vicinity of the discharge area within a waste rock pile and downstream of a nearby lake. The samples were subjected to chemical and isotopic analysis, with a focus on the potential for natural attenuation. The mine waste discharge has high initial concentrations of calcium, sulfate, and iron, and elevated concentrations of nickel, zinc, and strontium. These element concentrations are significantly reduced along the flow path so that the water is environmentally safe for discharge into the Loidlsee. The reduced contaminant levels are related to the formation of secondary iron precipitates and associated sorption processes, the formation of secondary calcium carbonates, and mixing with another groundwater source. The results indicate that the carbonate-dominated sediments of the Molasse zone contribute substantially to the natural remediation of a potential environmental problem.

Keywords: abandoned coal mines; Molasse zone; mining-influenced water; natural attenuation; Upper Bavaria

Academic Editors: Guang Li, Qinghai Deng and Jie Guo

Received: 7 March 2025
Revised: 11 April 2025
Accepted: 14 April 2025
Published: 23 April 2025

Citation: Hilberg, S.; Yousefi, N.; Rinder, T. Mining-Influenced Water from the Abandoned Hausham Colliery in Southern Germany—A Case of Unmonitored Natural Attenuation. *Water* **2025**, *17*, 1253. https://doi.org/10.3390/w17091253

1. Introduction

In the northern Alpine foreland, there are numerous lignite deposits in the Molasse Basin of Austria [1,2], southern Germany [3], and Switzerland [4]. Coal mining in Upper Bavaria, the focus of this study, was documented as early as the 16th century [5]. Mining continued until the 1960s, when further exploitation became economically unfeasible. The mines were closed and flooded. As was common in comparable coalfields at the time, no further attention was paid to mine water quality, and little is known about the environmental impact of the former mines. In recent decades, questions about mine water quality became an essential part of post-mining research, as evidenced by numerous studies [6–9]. It is well known that water quality might be influenced for decades after mining operations and can cause substantial environmental problems [10,11]. The environmental risks of coal mine drainage to surface and groundwater systems have been documented in numerous cases worldwide [12–14]. Depending on the mineralogical composition of the host rock and thus on the geological setting of the deposit, mine drainage may be acidic or neutral to alkaline [15]. Acid mine waters are produced by the contact of water and oxygen with

sulfides in the absence of buffering minerals. Circumneutral or alkaline mine waters occur where buffering minerals dominate the hydrochemical processes [16]. Negative impacts on water chemistry are often associated with acidification [17] and acid mine drainage is often an environmental concern in regions where sulfide ores have been mined [18,19]. Sulfides are also components of coal [20], and coal mine drainage around the world can contain problematic levels of harmful elements [8]. Mining itself disturbs the hanging wall rock sequence and exposes the rock to air, water, and microorganisms. In addition, all mined material can be a source of acidity once exposed to supergene processes. As a result, a number of studies have focused on the environmental influence of mine waste [21–23]. The remediation and prevention of environmental impacts associated with mining has become an important area of research [24,25], and a thriving sector of current mining technology.

Wolkersdorfer and Bantele carried out the first detailed investigations of mining-influenced water (MIW) in the Upper Bavarian Pechkohlenmulde (pitch coal basin) [26]. One of the adits investigated in their study was the so-called Wasserstollen in Hausham. The water chemistry was characterized by a relatively high electrical conductivity of 3474 µS/cm and elevated concentrations of arsenic, nickel, and zinc. Following these results, the aim of the current study is to evaluate the evolution of the MIW chemistry along the flow path between the mouth of the tunnel and the receiving lake Loidlsee. We want to understand whether this previously unmonitored mine water situation poses an environmental hazard or whether the geological situation is such that acid mine drainage is attenuated, and other problematic substances are also retained in the deposit area. The case study shows if and under what circumstances natural attenuation is sufficient to mitigate the risk of mining-related environmental hazards.

Field work was conducted in the summer of 2020. A coupled elemental and isotopic approach was used to reconstruct the origin and chemical evolution of the mine water. Water samples were collected along the mine water flow path and from surface waters in the immediate vicinity. In addition, solid samples of secondary mineral phases, sediments, and mine waste along the surface flow path were analyzed. Major and trace element compositions of solutions, solids, and water isotope ratios of $^{34}S/^{32}S$ and $^{18}O/^{16}O$ in sulfate and $^{18}O/^{16}O$, $^{2}H/^{1}H$ of H_2O were analyzed.

2. Materials and Methods

2.1. Study Area and Geological Setting

The study area is located in Bavaria, southern Germany, in the Molasse Basin, which extends between the Danube in the north and the Alps in the south. The basin is divided into the northern autochthonous foreland Molasse and the southern allochthonous folded Molasse zone. The sediments are the result of two transgression cycles of the Parathethys during the Oligocene and Miocene [27]. At that time, the climate was tropical with an average annual temperature of 20 °C and annual precipitation of 1600 to 1800 mm [28]. The region was characterized by alluvial fans with shallow water conditions and sea level fluctuations. In the transition zone between freshwater and marine sedimentation, organic sediments were deposited in great thickness and rapidly buried under younger sediments [29]. This led to optimal conditions for the formation of lignite deposits, known as pitch coal because of its luster. During the Alpine orogeny, the southernmost part of the molasse sediments was transported northwards and folded into syn- and anticlines running parallel to the northern edge of the Alps in an east–west direction [27]. During the progressive folding of the Alpine orogeny, the coal seams were buried deep under younger molasse sediments and their degree of coalification increased [30]. Today, the coal-bearing strata of the Bavarian pitch coal field are found in several synclines along the northern edge of the Alps between the Lech and Inn rivers [3].

The Hausham mine is located in the catchment area of the Leitzach and Mangfall rivers in the eastern part of the Upper Bavarian lignite mining area. The coal seams belong to the stratigraphically deepest units of the folded Molasse zone [31] and are interbedded with sandstones, marls, siltstones, claystones, and conglomerates. The sedimentary composition is dominated by carbonate components due to its origin in the Northern Calcareous Alps. Lignite contains five to seven percent sulfur, one-third of which is pyrite-bound [32].

During the mining, the excavated material was deposited on a mountain peak, the Brentenspitz. The resulting dump collapsed in the 1950s and buried Hausham colliery's water gallery. For this reason, there is currently no clearly identifiable mine water outlet. Water flows out of the dump and forms a small channel along the east side of the landslide material. Emerging mine water flows into the Loidlsee. This lake is the result of the damming of the east–west running Tiefenbach north of Hausham colliery by the landslide [33].

The data presented in this study were generated from samples collected at discharge points in the waste rock pile (MW 10 and MW 11), along the watercourse in the waste rock pile (MW 1 to MW 9), and at springs and watercourses in the Tiefenbach catchment not directly affected by mining (S 1, S 2, Li 1). Figure 1a shows the position of the study area in southern Germany (Upper Bavaria). The geological map and sampling sites are shown in Figure 1b, coordinates and further information about the hydrological connectivity between sampling points are given in Supplement Table S5_stations. Figure 1c,d shows sinter terraces in the lower part of the outcrop and iron ochre near the gallery. The delineation of the dump material was taken from the digital elevation model and verified during the field survey.

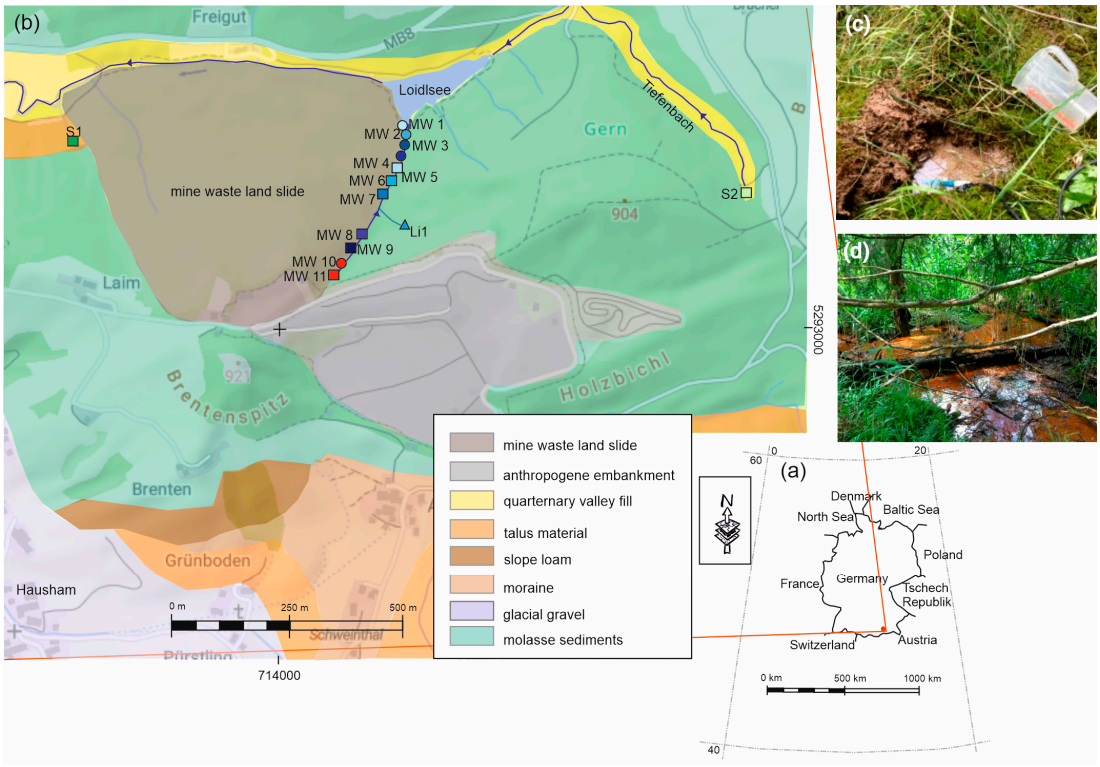

Figure 1. (**a**) Location of the Hausham mining area in Upper Bavaria on the northern edge of the folded Molasse zone. (**b**) Geological map of the study area with the collapsed spoil heap, the Loidlsee, the Tiefenbach catchment area and the water sampling points. Geology based on [34] (**c**) calcareous sinter under the grass on the mine dump. (**d**) Iron ochres in the vicinity of the MW 11 mine water outlet.

2.2. Sampling and Analysis

Based on the field survey and the digital elevation model, a 1:10,000 scale geological–hydrogeological map was prepared showing the location of springs and mine water outlets. Fourteen water samples were taken in August 2020. Electrical conductivity, dissolved oxygen, temperature, and pH were measured with a WTW 350i ProfiLine Multi 3320 multiparameter handheld meter (Xylam Analytics GmbH, Weilheim, Germany) (probes: EC TetraCon 325, pH SenTix 41, O_2 CellOx 325). Oxygen and pH sensors were calibrated in the field immediately prior to measurements. All samples were filtered through 0.45 µm regenerated cellulose filters and stored in gas-tight Duran glass bottles (150 mL) for alkalinity measurements and 125 mL HDPE Nalgene bottles (rinsed three times with sample water) for chemical analyses. Samples for cation analyses were acidified to pH ≈ 2 with concentrated HNO_3 (Merck ultrapure) (Merck KGaA, Darmstadt, Germany). Samples were placed in a cooler, transported to the laboratory, and stored refrigerated.

Alkalinity was measured by potentiometric titration with HCl 0.01N (Titroline 5000) (Mettler-Toledo GmbH, Vienna, Austria) one day after sampling at the hydrogeology laboratory of the Paris Lodron University of Salzburg, Austria. Ion chromatography and ICP-OES measurements were performed at the Graz University of Technology, Austria. Concentrations of dissolved cations (Na^+, K^+, Mg^{2+}, Ca^{2+}) and anions (Cl^-, NO^{3-}, $SO_4{}^{2-}$, and Br^-) were determined by ion chromatography using a Dionex ICS-3000 (ThermoFisher Scientific GmbH, Vienna, Austria). Chemical analyses of trace elements (Ag, Al, Ba, Bi, Fe, Ga, In, Li, Mn, Ni, Si, Sr, Zn, and As) were performed by ICP-OES (Perking Elmer OPTIMA 8300 DV) (Perkim Elmer, Inc., Waltham, USA) with analytical precision better than ±5% based on replicate analyses of selected samples (n = 2). Data interpretation and visualization were performed using AquaChem 12.0 software [35]. The hydrochemical code PHREEQC [36], as an integrated tool in AquaChem 12.0 [35], was used to calculate saturation indices (SIs). For data processing, the thermodynamic database phreeqC.dat based on the ion dissociation theory [37] was integrated into AquaChem.

The isotope values of the waters were analyzed by wavelength-scanned cavity ring-down spectroscopy (WS-CRDS) using a Picarro L1102-i system (Picarro, Inc., Santa Clara, Canada). The analytical procedure of the WS-CRDS measurements is similar to the method described by the authors of [38]. Typical analytical precisions (1 σ) are ±1 ‰ for δ^2H and ±0.08 ‰ for $\delta^{18}O$, and values are referenced to the Vienna standard mean ocean water (V-SMOW) standard. Analysis of $^{34}S/^{32}S$ ratios in sulfate was performed at Imprint Analytics GmbH (Neutal, Austria) (applied methods: 03.001EA-IRMS (05-2022) for $\delta^{34}S$, 03.002 HTO-IRMS (04-2018) for $\delta^{18}O$). $^{18}O/^{16}O$ ratios were determined by the same laboratory using a Hekatech TCEA coupled to the NU Horizon IRMS. Isotopic analyses of sulfur and oxygen in sulfate and hydrogen and oxygen in water are reported in δ notation relative to a standard (VCDT for sulfate, V-SMOW for oxygen and hydrogen).

Solids from stream sediments, sinter terraces, iron ochres, and dump material were collected directly from the surface as single or mixed samples using a hand shovel. The elemental composition of the solids (n = 5) was analyzed using an "S4 Pioneer" X-ray fluorescence microscope (BrukerAXS, Billerica, USA). This instrument is equipped with a 4 kW X-ray tube, with the major elements measured at reduced power. Counting times were chosen so that the double standard deviation was less than 1% (relative) for SiO_2 and Al_2O_3, and less than 5% (relative) for the elements containing 1–10%. At low element contents (<10 mg/kg), the measurement error is typically 1–3 mg/kg. At levels around 1000 mg/kg, the errors are 50 mg/kg maximum, but for many trace elements they are much

lower. Trace element concentrations have been interpreted using the geo-accumulation index approach [39,40] using the following equation:

$$I_{geo} = \ln[w_i/(1.5 \times B_i)] \quad (1)$$

I_{geo}: geo-accumulation index [40],
w_i: measured mass fraction of chemical elements in the solids [mg/kg],
B_i global geochemical background [mg/kg] [41].
The evaluation of results is done according to the classification in Table 1.

Table 1. Geo-accumulation index classification. The geo-accumulation index (I_{geo}) represents the extent of enrichment of a parameter compared to the global average according to Turekian and Wedepohl [41].The index class is the numerical description of the extent of contamination [39,40].

I Geo	Index Class	Contamination Intensity
>5	6	very strong
>4–5	5	strong to very strong
>3–4	4	strong
>2–3	3	moderate to strong
>1–2	2	moderate
>0–1	1	uncontaminated to moderate
<0	0	uncontaminated

Leaching experiments (n = 4) were performed with material collected as composite samples from the waste rock material, carbonate sinters, and iron ochres with a grain size <32 mm in a 1:10 weight ratio with deionized water. Samples were shaken at one rotation per minute for 24 h prior to filtration and acidification for analysis. The eluate was analyzed by IC (major elements) and IC-OES (trace elements) according to the water analysis methods described above.

3. Results and Discussion

3.1. Geological and Hydrogeological Setting

A 1:10,000 scale map of the project area was prepared based on field observations and the digital elevation model [42]. The map in Figure 1b shows the delineation of the stockpile and its surroundings. The dump material covers an area of 314,230 m^2. The main surface water bodies are the Loidlsee and the Tiefenbach stream. A small stream flows towards the Loidlsee on the eastern side of the stockpile. This watercourse collects all diffuse water outlets and channels from the landslide area. From the presumed level of the buried "Wasserstollen" downwards, numerous small channels flow over the dump, sometimes seeping into the ground and emerging again. Iron ochre deposits have formed where the water first reaches the surface (Figure 1c). Further downstream a network of small channels, massive carbonate precipitation, and sinter terrace formation can be observed (Figure 1d). In addition to two apparent initial mine water outflows in the upper part of the dump (MW 10 and MW 11), a lateral inflow (Li 1) was identified to the east of the pile. The Tiefenbach catchment was sampled to its head spring approximately 1 km east of Loidlsee, and the spring (S 2) was included in the sampling program as a local reference. An additional spring (S 1) was mapped and sampled in the Tiefenbach ditch to the west (i.e., orographically below) of the dump. Solid samples for geochemical analysis were collected at stations MW 2, MW 6, MW 11, and Li 1. Stream sediments were collected as a composite sample from the entire stream between MW 11 and MW 1. Samples for eluate analysis were collected as composite samples from the waste rock pile material as

well as from various calcareous sinter and iron ochre deposits throughout the waste rock pile area.

3.2. Hydrochemical Characterization

Chemical and isotope data of all water samples are provided as Supplemental Material (Table S1_solutions), and an overview of the most important results is shown in Table 2. According to the local geology, the chemical composition of the local waters is mostly determined by calcium carbonate dissolution, which is consistent with the average chemical composition of the region according to a study by Wagner et al. [43]. Based on their origin and chemical signature, the waters were classified into the following four groups (Figure 2): (1) local reference waters, (2) lateral inflow, (3) mining influenced waters along the flow path, and (4) waters directly discharged from the adit.

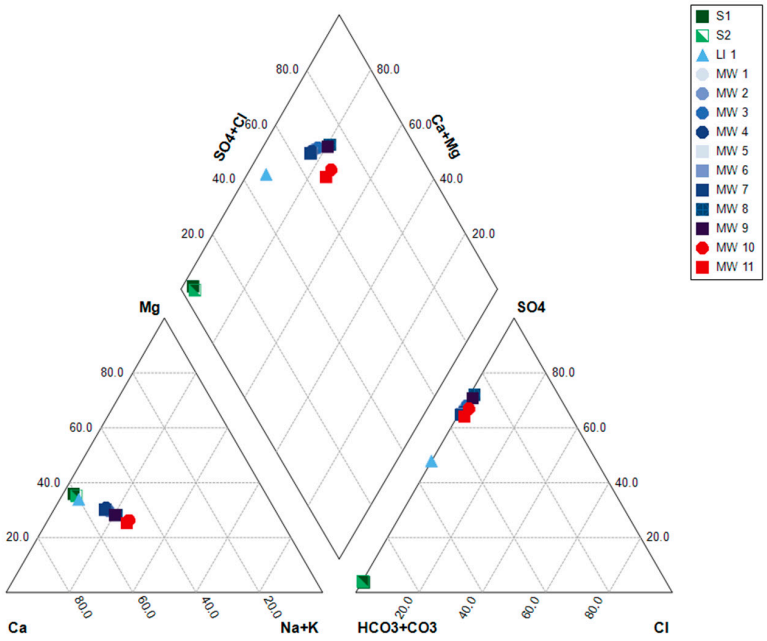

Figure 2. Major element composition of (1) local reference waters with Ca-HCO_3 dominated composition (green rectangles; S 1–S 2); (2) lateral inflow with Ca-HCO_3-SO_4 water type (light blue triangle; Li 1); (3) mining influenced waters along the flow path (dark blue symbols; MW 1–MW 9); and (4) Ca-SO_4 waters directly from the adit (red symbols; MW 10–MW 11). The Piper plot shows the percentage distribution and allows the waters to assign to the specific water types according to [44].

Table 2. Overview of field parameters, major ion composition, and the three most important trace parameters. The complete analysis data set is documented in Supplement Table S1_solutions.

Sample	pH	Cond.	Na	K	Mg	Ca	Cl	SO_4	HCO_3	Sr	Ni	Zn
		µS/cm	mmol/L	mmol/L	mmol/L	mmol/L	mmol/L	mmol/L	mmol/L	µmol/L	µmol/L	µmol/L
S 1	8.31	458	0.150	0.043	1.001	1.681	0.045	0.088	4.823	1.785	0.096	0.024
S 2	8.35	532	0.285	0.036	1.206	2.046	0.024	0.122	6.130	2.904	0.099	0.036
Li 1	7.78	1017	0.574	0.201	2.130	3.756	0.017	2.824	6.185	20.775	<0.085	0.026
MW 1	8.40	1490	2.704	0.436	2.831	4.865	0.201	5.856	5.675	36.899	<0.085	0.027
MW 2	8.27	1497	2.714	0.440	2.837	4.912	0.198	5.865	5.695	37.060	0.090	0.016
MW 3	8.12	1568	2.977	0.487	2.923	5.155	0.234	6.282	5.712	39.584	<0.085	0.027
MW 4	8.13	1458	2.553	0.422	2.799	4.801	0.186	5.615	5.747	35.177	<0.085	0.029
MW 5	8.34	1500	2.653	0.439	2.873	5.028	0.193	5.792	6.063	37.611	0.090	0.020
MW 6	8.15	1513	2.669	0.442	2.890	5.102	0.195	5.825	6.154	34.790	<0.085	0.022
MW 7	7.96	1524	2.678	0.442	2.891	5.105	0.197	5.829	6.181	36.986	<0.085	0.034
MW 8	8.15	1972	4.748	0.690	3.715	6.645	0.385	8.804	6.509	53.565	0.112	0.035
MW 9	7.99	2040	4.789	0.707	3.799	6.896	0.404	8.910	6.985	54.859	0.102	0.029
MW 10	7.38	2830	8.482	1.149	4.913	8.920	0.889	11.752	10.833	79.361	0.192	0.039
MW 11	6.90	2710	7.862	1.083	4.463	8.639	0.786	10.798	11.371	76.773	0.179	0.038

The waters can be classified according to their calcium/magnesium ratios to obtain information about the mineral phases and dissolution processes in the catchment area. Figure 3a shows a clear positive correlation between calcium and magnesium with a ratio in the range of 2:1 (a ratio of 1:1, represented by the gray dashed line in Figure 3a would indicate pure dolomite dissolution). Although this is in good agreement with the carbonate sediments of the molasse zone (calcite and dolomite sediments from the Northern Calcareous Alps), the comparatively low correlation with hydrogen carbonate (Figure 3b) indicates that other mineral dissolution processes must play a substantial role in the genesis of the water. The ratio of 1:1, shown as gray dashed line in Figure 3b, would indicate carbonate dissolution as the only origin of the observed water composition. A significant increase in calcium and magnesium mineralization between reference water and mine water and a gradual decrease in the concentrations with increasing distance from the mine water outlets can be observed (Figure 4b). This indicates that carbonate dissolution by circulating groundwater in the catchment is the dominant factor, but that this process must be superimposed by another weathering process in the mine-influenced area. Evidence for mining-related dissolution processes can be seen from the relatively weak correlation of calcium plus magnesium vs. hydrogen carbonate (Figure 3b) and a strong correlation of the sum of cations (calcium, magnesium, potassium, and iron) vs. sulfate (Figure 3c). The 1:1 line in Figure 3c represents a process of sulfate dissolution. The ratio of (alkaline earth) metals to sulfate is shifted in parallel in favor of metals, while the reference waters are almost free of sulfate, indicating that the mining influence causes the sulfate and metal concentrations to increase. Sulfate concentration in the mine waters could generally be due to either evaporite or sulfide dissolution. If gypsum solutions were the determining process, the water would have a Ca/SO_4 ratio of 1:1 (represented by the gray dashed line in Figure 4d). The calculation of pyrite-driven calcite dissolution (at a P_{CO2} of $10^{-2.5}$ which is in the range of the mine waters as documented in Supplement Table S2_isotope_SI) is plotted in Figure 3d (black dashed line). The fact that the mine waters plot on this black dashed line demonstrates that sulfide-driven carbonate dissolution is an essential process in the genesis of the mine waters.

The evolution of the major element concentrations along the flow path between the mine water outflow and the inflow into the Loidlsee shows that significant changes occur at two points. (1) After the discharge of the mine waste, CO_2 degassing occurs gradually between MW 11 and MW 8 (Figure 4a) and leads to the precipitation of calcite (Supplement Table S3_solids). This is indicated by a decrease in calcium and hydrogen carbonate (Figure 4b) and can be seen in the field as massive calcite sinter deposits (Figure 1d). In addition, exposure to air results in the immediate precipitation of iron hydroxides. This is evidenced by a significant decrease in iron concentrations from 0.05 mmol/L in MW 10 to <0.001 mmol/L in MW 9, and by iron hydroxide precipitation only in the uppermost part of the flow path (Figure 1c). (2) Lateral inflow (Li1) between MW 8 and MW 7 results in mixing and thinning of the much higher mineralized MIW. The sulfate concentration also decreases significantly between MW 10 and MW 8. Unlike the Ca-carbonates, this cannot be explained by precipitation of mineral phases. As can be seen in the Supplement Table S3_solids, SO_3 only appears to a lesser extent in the analyzed precipitates. Figure 4c shows that the water at each station is clearly undersaturated with respect to gypsum. Dolomite precipitation is unlikely in the modern environment due to kinetic barriers regardless of its saturation state [45]. The decrease in magnesium and sulfate is therefore exclusively due to dilution with sulfate-free and lower mineralized ground or surface water. This is particularly evident after the injection of Li 1. After mixing with Li 1, the major ion composition of MIW remains constant until it enters the lake.

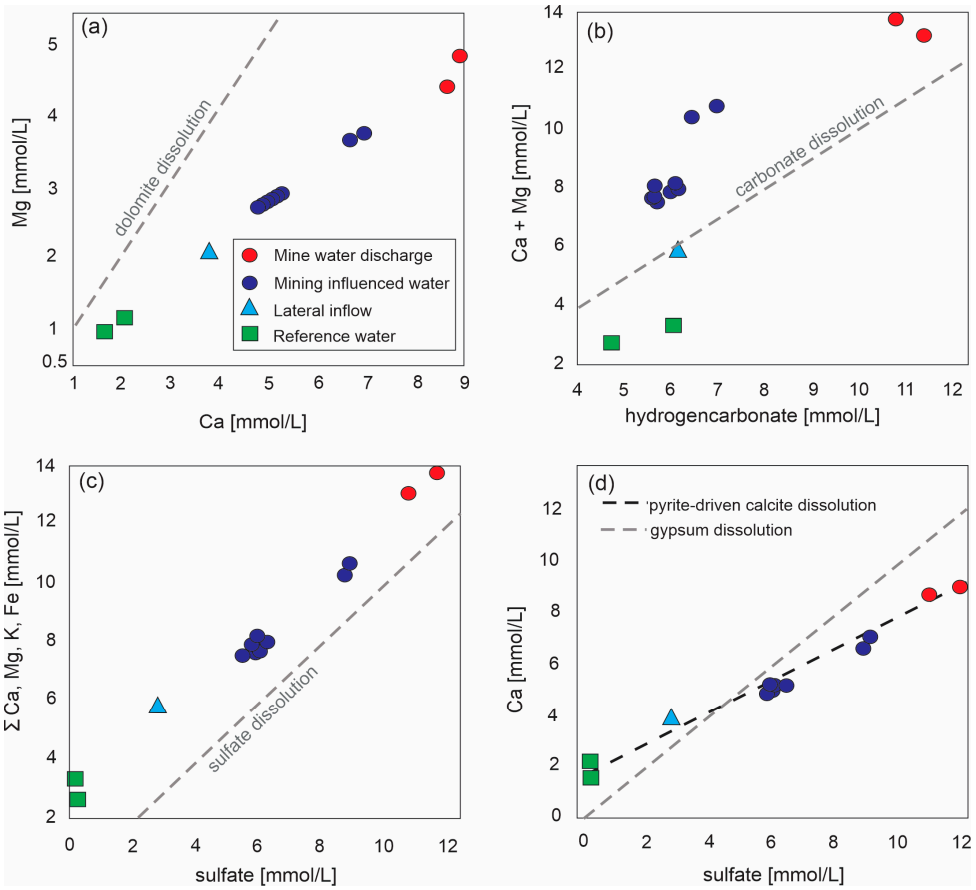

Figure 3. Scatter plots showing the correlation between (**a**) Ca/Mg, (**b**) Ca+Mg/HCO_3, (**c**) Ca+Mg/SO_4, and Ca/SO_4. Gray lines represent the 1:1 lines, the black dashed line in (**d**) represents the chemical evolution of reference water S 1 with the simultaneous dissolution of calcite and the stepwise dissolution of pyrite at P_{CO2} of $10^{-2.5}$, modeled with PHREEQC.

The complete trace element composition is documented in Supplement Table S1_solutions. Trace elements with considerable concentrations are shown again along the flow path in Figure 4d. In agreement with the site results, iron is only measurable in the immediate vicinity of the discharge. Strontium, nickel, and zinc concentrations also decrease between MW 10 and MW 9. After discharge of the dump, these trace elements are efficiently removed from the water. In the case of strontium, it can be assumed that this is due to either strontianite precipitation or incorporation into the calcite sinter. The chemical composition of the carbonate sinter confirms that strontium is incorporated into the calcite deposits while nickel and zinc are probably adsorptively enriched in the stream sediments and incorporated into iron ochres (Supplement Table S3_solids). Figure 4c shows that strontianite is slightly supersaturated in MW 11 and MW 10 and undersaturated from MW 9 downward. Celestite, on the other hand, is always undersaturated, i.e., there is no strontium sulfate precipitation. Another interesting observation shown in Figure 4d is the increase in barium between MW 10 and MW 9. Here, the concentration rises due to the lateral inflow and shows comparatively high values in the two reference waters, and it can be assumed that this is a local geogenic background value and not caused by mining.

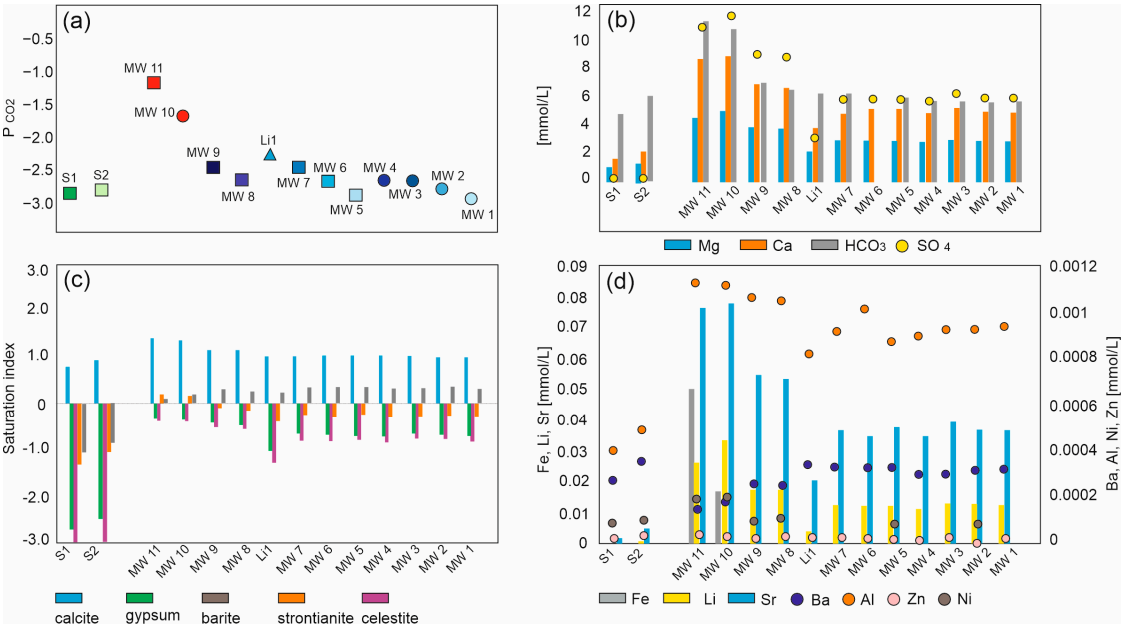

Figure 4. Hydrochemical evolution along the flow path. A compilation of all major and trace element analyses and calculated saturation indices can be found in Supplement Tables S1 and S2. (**a**) CO_2 partial pressure (shown as P_{CO2}), equilibrium with the atmosphere (0.04 Vol%, $P_{CO2} = -3.4$) is not reached along the flow path to the lake. (**b**) Major ion concentrations. (**c**) Saturation indices (SIs) of mineral phases that are either highly supersaturated or show notable changes along the flow path. Dolomite is always highly supersaturated, but changes little along the flow path and is therefore not shown. (**d**) Trace element composition, only the elements that are clearly above the detection limit are shown.

3.3. Water Isotope Signature

In terms of the $\delta^{18}O/\delta^{2}H$ ratio, all waters are close to the local meteoric waterline (LMWL) based on data from the GNIP station Hohenpeißenberg [46] (Figure 5). This shows, first, that the water is all meteoric and that there are no evaporation effects or influences from formation water. Comparing the measured isotope signatures with monthly precipitation data, the sampled waters are in the range of spring or fall precipitation (Figure 5). This indicates an average residence time of three to four months for the August samples.

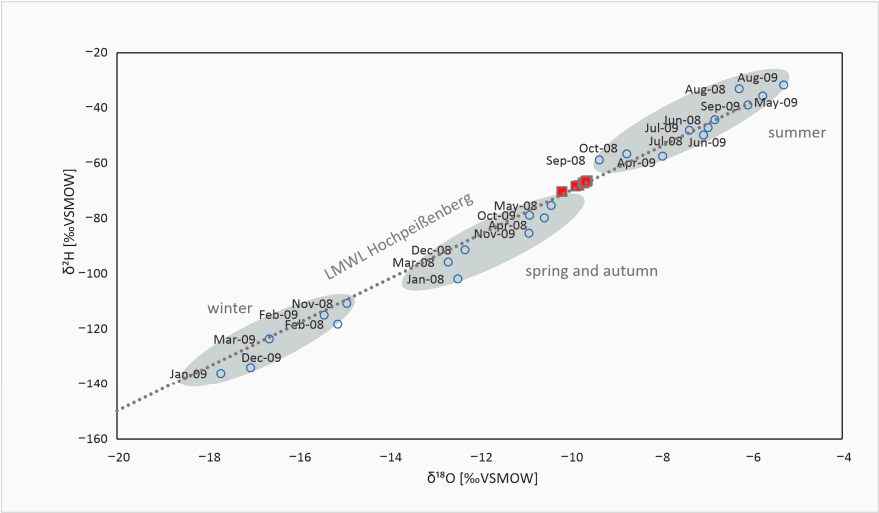

Figure 5. $\delta^{18}O$ v.s $\delta^{2}H$ of the water samples (August 2020) and precipitation values (2008, 2009) of the GNIP (global network of isotope in precipitation) station Hochpeißenberg and LMWL (local meteoric water line) Hochpeißenberg [47]. Full isotope data set is provided in Supplement Table S2_Isotope_SI.

The sulfate molecule (SO_4^{2-}) can contain different isotopes of both sulfur and oxygen. The most common isotope of sulfur is ^{32}S and that of oxygen is ^{16}O. There is also the presence of the heavy isotopes ^{34}S and ^{18}O, each with two extra neutrons in the nucleus. Isotopes of the same element have the same chemical but different physical properties. As a result, the ratio of light to heavy isotopes changes during physical processes. This can be used to trace the origin of sulfate in various hydrogeological settings [48–51] and specifically in the context of MIW [14,52]. Sulfate associated with gypsum and calcite is generally isotopically heavier than sulfate from pyrite oxidation [53,54]. As shown in Figure 6, the isotopic composition of the waters is typical of sulfate from pyrite oxidation for MIWs, lateral inflows, and stream waters. However, the potentially non-influenced spring waters S 1 and S 2 also plot in the sulfide oxidation range (Figure 6). The total sulfate concentrations in both samples are very low (Figure 4b) and there is no evidence of gypsum dissolution in the catchment. Therefore, it can be assumed that the mining activity also influences these sampling points to a lesser extent. It is noticeable that the Tiefenbach spring (S 2) and the lateral inflow (Li 1), for which no mining influence is assumed, have the lightest sulfate isotopes, while the second reference spring (S 1) to the west of the mine dump has the comparatively heaviest sulfate isotope signature of all sampled waters.

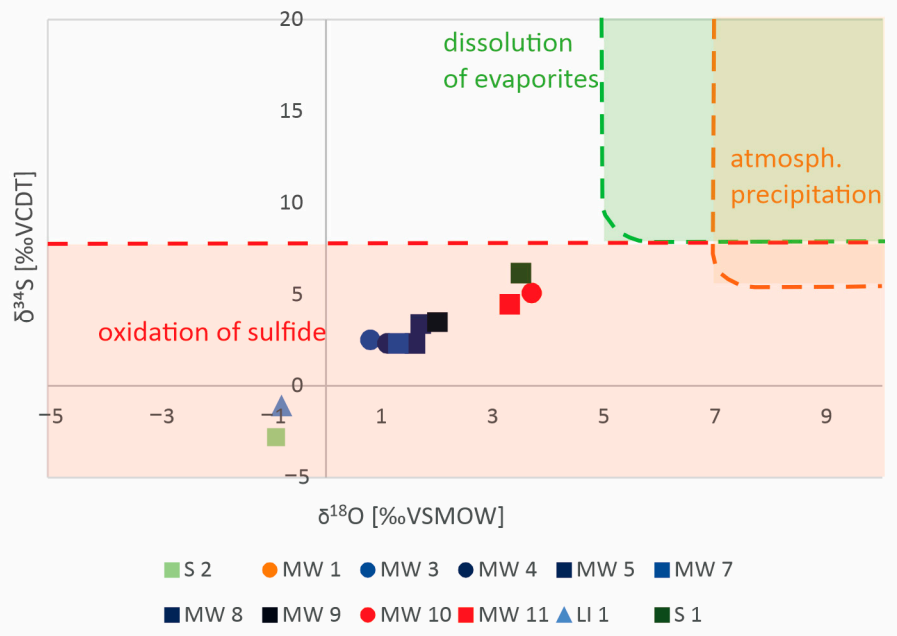

Figure 6. Sulfate $\delta^{18}O$ vs. $\delta^{34}S$ in water samples. Process area delineation based on data from Wang and Zhang [54]. All data, including the two reference waters S 1 and S 2, for which no direct mine water influence is expected, plot in the sulfide oxidation field. $\delta^{18}O$ and $\delta^{34}S$ values are positively linearly correlated.

3.4. Geochemical Composition of Solids and Eluates

Iron ochre from the mine water discharge (locality MW 11), calcium carbonate sinter from the mine drainage (MW 2, MW 6) and lateral inflow (Li 1), and a sample of sediment from the riverbed were analyzed for chemical composition (Supplement Table S3_solids). Trace element concentrations were classified using the geo-accumulation index [39,40] based on global background values according to Turekian and Wedepohl [41]. Iron ochres and river sediments were compared to the sand standards, calcareous sinters to the carbonate standard to calculate the indices and evaluate the contamination intensity. As shown in Table 3, concentrations of potentially hazardous metals in the river sediments and iron ochres are classified as strong while the contamination of carbonate sinters is

classified as moderate. The highest contamination was found for arsenic, nickel, strontium, and uranium.

Table 3. Mass fraction and assessment of potentially environmentally hazardous trace elements in solids. Analytical data were compared with global standards for sands (sediments and iron ochres) and carbonates (sinters) according to Turekian and Wedepohl [41] and evaluated according to Müller [40]. Index classification according to Gupta et al. [39].

Sample	Sediment	Sinter MW 6	Sinter MW 2	Sinter Li 1	Fe Ochre MW 11	Standard Sand	Standard Carbonate
As (mg/kg)	31	bdl	5	bdl	76	1	1
Ba (mg/kg)	612	bdl	bdl	bdl	268	0	10
Cr (mg/kg)	188	66	78	49	58	35	11
Ni (mg/kg)	120	49	43	38	76	2	20
Sr (mg/kg)	899	3970	3359	2984	2495	20	610
U (mg/kg)	54	22	22	16	41	0	2
Zn (mg/kg)	161	73	56	25	125	16	20
I_{geo} As	3.0		1.3		3.9		
I_{geo} Ba							
I_{geo} Cr	1.3	1.4	1.5	1.1	0.1		
I_{geo} Ni	3.7	0.5	0.4	0.2	3.2		
I_{geo} Sr	3.4	1.5	1.3	1.2	4.4		
I_{geo} U	4.4	1.9	1.9	1.6	4.1		
I_{geo} Zn	1.9	0.9	0.6	−0.2	1.6		
I_{geo} mean	3.2	1.4	1.3	1.1	3.6		
Index class	4	2	2	2	4		

The metal contents are highest in the sediment, but the iron ochres and to some extent the calcium carbonates also bind some of these metals. A comparison with the concentrations of trace elements in the water samples, using nickel and zinc as examples (Figure 4), shows that the waters become depleted with increasing distance from the discharge, while the iron hydroxides and the sediment, and to a lesser extent the calcareous sinter, absorb and thus demobilize these trace elements.

To verify that this demobilization in secondary minerals is sustainable, four samples (one calcareous sinter, one sediment sample from the flow path, and two samples from the waste rock pile) were collected for eluate analysis (analytical results in Supplement Table S4 leaching experiments). The samples were pooled from several individual sampling locations and therefore do not correspond to any of the water sampling locations. In general, none of the potentially problematic elements showed strong leaching behavior after 24 h. Leaching was lowest in the sintered material, demonstrating effective ion retention. This is evidenced by the strontium content, which ranged from 1.3 to 1.7 mg/L in the waste rock samples but only 0.3 mg/L in the sinter sample. However, the correlation is less clear when the parameters nickel and zinc are considered.

4. Conclusions

Mixing sulfide mine waste with other materials has been proposed as a potential strategy to mitigate the negative effects of mine water discharge. The case study presented provides a good natural example of the effectiveness of this approach. Our results show that carbonate waste rock, in a suitable spatial connection to the mine drainage, can contribute to the purification of the mine water. Since the incorporation of trace elements is different for iron oxides and calcium carbonates, the spatial decoupling of these two secondary precipitation products concentrates the individual elements in their respective phases. This could be advantageous for potential future reuse of waste rock material and help to significantly reduce the costs associated with remediation.

The situation at Hausham is unique due to the landslide. Nevertheless, the geological situation and the generally carbonate-dominated catchment area are very comparable to countless previously unmonitored mine water discharges from historic mines in the Molasse zone throughout Central Europe. Therefore, a cautiously positive assessment of the mining-influenced waters in the region can be derived from our results.

Supplementary Materials: The following supporting information can be downloaded at: https://www.mdpi.com/article/10.3390/w17091253/s1, Table S1: solutions; Table S2: isotope_SI, Table S3: solids, Table S4: leaching experiments, Table S5: stations.

Author Contributions: Conceptualization, T.R.; methodology, T.R. and S.H.; validation, S.H.; investigation, N.Y., T.R. and S.H.; resources, S.H.; data curation, S.H.; writing—original draft preparation, T.R.; writing—review and editing, S.H.; visualization, S.H. and N.Y.; supervision, S.H.; project administration, S.H.; funding acquisition, S.H. All authors have read and agreed to the published version of the manuscript.

Funding: This research was funded by the Foundation Forum Bergbau und Wasser in the Stifterverband für die Deutsche Wissenschaft e.V., grant number: T0518/30384.

Data Availability Statement: All data generated in this study can be found in the Supplemental Material.

Acknowledgments: We thank David Schiller and Fritz Finger for providing RFA analyses. Thanks to anonymous reviewers of a former and the current version of this manuscript for their valuable comments and suggestions. They strongly helped to revise the article.

Conflicts of Interest: When the study presented here was carried out, the author Thomas Rinder was employed as a Postdoc at the University of Salzburg and was funded by the Foundation Forum Bergbau und Wasser (see Funding informtion above). He is now employed by the company AFRY Austria GmbH, which has no connection with the study presented here. All authors declare that the research was conducted in the absence of any commercial or financial relationships that could be construed as a potential conflict of interest.

References

1. Groiss, R. Geologie und Kohlebergbau im Hausruck (Oberösterreichische Molasse). *Arch. Für Lagerstättenforschung* **1989**, *11*, 167–178.
2. Weber, L.; Weiß, A. *Bergbaugeschichte und Geologie der österreichischen Braunkohlenvorkommen*; Geologische Bundesanst: Wien, Austria, 1983; ISBN 3900312265.
3. Müller, M. Die Oberbayerische Pechkohle: Die Fortsetzung oligozäner und miozäner Kohlevorkommen aus der Faltenmolasse in die oberbayerische Vorlandmolasse. *Geol. Bavarica* **1975**, *73*, 113–121.
4. Sachsenhofer, R.F.; Aghayeva, V.; Ajuaba, S.; Kojić, I.; Misch, D.; Stojanović, K. Horgen-Käpfnach, the largest Swiss coal deposit: Geology, petrology and geochemistry. *Int. J. Coal Geol.* **2025**, *299*, 104684. [CrossRef]
5. Balthasar, K. Die Oberbayerische Pechkohle: Geschichte und Bergtechnik der Kohlebergwerke Penzberg und Hausham. *Geol. Bavarica* **1975**, *73*, 7–24.
6. Burke, S.P.; Younger, P.L. Groundwater rebound in the South Yorkshire coalfield: A first approximation using the GRAM model. *Q. J. Eng. Geol. Hydrogeol.* **2000**, *33*, 149–160. [CrossRef]
7. Burrows, J.E.; Peters, S.C.; Cravotta, C.A. Temporal geochemical variations in above- and below-drainage coal mine discharge. *Appl. Geochem.* **2015**, *62*, 84–95. [CrossRef]
8. Gombert, P.; Sracek, O.; Koukouzas, N.; Gzyl, G.; Valladares, S.T.; Frączek, R.; Klinger, C.; Bauerek, A.; Areces, J.E.Á.; Chamberlain, S.; et al. An Overview of Priority Pollutants in Selected Coal Mine Discharges in Europe. *Mine Water Environ.* **2019**, *38*, 16–23. [CrossRef]
9. Kessler, T.; Mugova, E.; Jasnowski-Peters, H.; Rinder, T.; Stemke, M.; Wolkersdorfer, C.; Hilberg, S.; Melchers, C.; Struckmeier, W.; Wieber, G.; et al. Grundwasser in ehemaligen deutschen Steinkohlenrevieren—Ein wissenschaftlicher Blickwinkel auf Grubenflutungen. *Grundwasser* **2020**, *25*, 259–272. [CrossRef]
10. Sengupta, M. *Environmental Impacts of Mining: Monitoring, Restoration, and Control*, 2nd ed.; CRC Press: Boca Raton, FL, USA, 2021; ISBN 9781003164012.

11. Wolkersdorfer, C. *Water Management at Abandoned Flooded Underdground Mines—Fundamentals, Tracer Tests, Modelling, Water Treatment*; Springer: Berlin/Heidelberg, Germany, 2008.
12. Banks, D.; Younger, P.L.; Arnesen, R.-T.; Iversen, E.R.; Banks, S.B. Mine-water chemistry: The good, the bad and the ugly. *Env. Geol* **1997**, *32*, 157–174. [CrossRef]
13. Cravotta, C.A. Dissolved metals and associated constituents in abandoned coal-mine discharges, Pennsylvania, USA. Part 1: Constituent quantities and correlations. *Appl. Geochem.* **2008**, *23*, 166–202. [CrossRef]
14. Rinder, T.; Dietzel, M.; Stammeier, J.A.; Leis, A.; Bedoya-González, D.; Hilberg, S. Geochemistry of coal mine drainage, groundwater, and brines from the Ibbenbüren mine, Germany: A coupled elemental-isotopic approach. *Appl. Geochem.* **2020**, *121*, 104693. [CrossRef]
15. Nordstrom, D.K. Mine Waters: Acidic to Circmneutral. *Elements* **2011**, *7*, 393–398. [CrossRef]
16. Younger, P.L.; Robins, N.S. Challenges in the characterization and prediction of the hydrogeology and geochemistry of mined ground. *Geol. Soc. Lond. Spéc. Publ.* **2002**, *198*, 1–16. [CrossRef]
17. Acharya, B.S.; Kharel, G. Acid mine drainage from coal mining in the United States—An overview. *J. Hydrol.* **2020**, *588*, 125061. [CrossRef]
18. Balci, N.; Shanks, W.C.; Mayer, B.; Mandernack, K.W. Oxygen and sulfur isotope systematics of sulfate produced by bacterial and abiotic oxidation of pyrite. *Geochim. Cosmochim. Acta* **2007**, *71*, 3796–3811. [CrossRef]
19. Gao, M.; Tang, J.; Tu, Y.; Zhu, M.; Nie, Z.; Liu, X.; Liu, G. The response and ecological implications between various sulfur forms and environmental factors in acid mine drainage. *Environ. Res.* **2025**, *275*, 121425. [CrossRef]
20. Chou, C.-L. Sulfur in coals: A review of geochemistry and origins. *Int. J. Coal Geol.* **2012**, *100*, 1–13. [CrossRef]
21. Alvarez, E.; Fernández Marcos, M.L.; Vaamonde, C.; Fernández-Sanjurjo, M.J. Heavy metals in the dump of an abandoned mine in Galicia (NW Spain) and in the spontaneously occurring vegetation. *Sci. Total Environ.* **2003**, *313*, 185–197. [CrossRef]
22. Dang, Z.; Liu, C.; Haigh, M.J. Mobility of heavy metals associated with the natural weathering of coal mine spoils. *Environ. Pollut.* **2002**, *118*, 419–426. [CrossRef]
23. Qureshi, A.; Maurice, C.; Öhlander, B. Potential of coal mine waste rock for generating acid mine drainage. *J. Geochem. Explor.* **2016**, *160*, 44–54. [CrossRef]
24. Moodley, I.; Sheridan, C.M.; Kappelmeyer, U.; Akcil, A. Environmentally sustainable acid mine drainage remediation: Research developments with a focus on waste/by-products. *Miner. Eng.* **2018**, *126*, 207–220. [CrossRef]
25. Naidu, G.; Ryu, S.; Thiruvenkatachari, R.; Choi, Y.; Jeong, S.; Vigneswaran, S. A critical review on remediation, reuse, and resource recovery from acid mine drainage. *Environ. Pollut.* **2019**, *247*, 1110–1124. [CrossRef] [PubMed]
26. Wolkersdorfer, C.; Bantele, M. Die Oberbayerische Pechkohlenmulde—Hydrogeochemische Untersuchungen der Grubenwässer. *Grundwasser* **2013**, *18*, 185–196. [CrossRef]
27. Berge, T.B.; Veal, S.L. Structure of the Alpine foreland. *Tectonics* **2005**, *24*, TC5011. [CrossRef]
28. Barthelt, D. Faziesanalyse und Untersuchungen der Sedimentationsmechanismen in der Unteren Brackwasser-Molasse Oberbayerns. In *Münchner Geowissenschaftliche Abhandlungen*; ConchBooks: Harxheim, Germany, 1989; pp. 1–118.
29. Geissler, P. Die Oberbayerische Pechkohle: Zur Geologie im Ostfeld des Kohlebergwerks Peißenberg. *Geol. Bavarica* **1975**, *73*, 55–106.
30. Teichmüller, M.; Teichmüller, R. Die Oberbayerische Pechkohle: Inkohlungsuntersuchungen in der Molasse des Alpenvorlandes. *Geol. Bavarica* **1975**, *73*, 123–142.
31. Lensch, G.; Wolf, M.; Brunnacker, K. *Stratigraphie, Fazies und Kleintektonik der kohleführenden Schichten in der bayerischen Faltenmolasse: (Peissenberg, Peiting, Penzberg, Hausham, Marienstein). Sporenstratigraphische Untersuchungen in der gefalteten Molasse der Murnauer Mulde*; Bayerisches Geologisches Landesamt: Oberbayern, Germany, 1961.
32. Pinsl, L. Die Oberbayerische Pechkohle: Chemische Kennzeichen der Oberbayerischen Glanzbraunkohle in den Bergwerken Peißenberg und Peiting. *Geol. Bavarica* **1975**, *73*, 107–111.
33. BVF Miesbach-Tegernsee. Bezirksfischereiverein Miesbach-Tegernsee: Gewässer. Available online: https://bfv-mbteg.de/gewasser/loidlsee/ (accessed on 19 February 2025).
34. Bayerisches Landesamt für Umwelt. Umweltatlas: Geologische Karte 1:25.000, Blatt 8236 Tegernsee. Available online: https://www.umweltatlas.bayern.de/mapapps/resources/apps/umweltatlas/index.html?lang=de&dn=lfu_domain-geologie (accessed on 28 February 2025).
35. Waterloo Hydrogeologic. *AquaChem*; Waterloo Hydrogeologic: Waterloo, ON, Canada, 2022.
36. Parkhurst, D.L.; Appelo, C.A.J. *Description of Input and Examples for PHREEQC Version 3: A Computer Program for Speciation, Batch-Reaction, One-Dimensional Transport, and Inverse Geochemical Calculations*; U.S. Department of the Interior, U.S. Geological Survey: Reston, VA, USA, 2013.
37. Debye, P.; Hückel, E. Zur Theorie der Elektrolyte. *Phys. Z.* **1923**, *24*, 185–206.

38. Brand, W.A.; Geilmann, H.; Crosson, E.R.; Rella, C.W. Cavity ring-down spectroscopy versus high-temperature conversion isotope ratio mass spectrometry; a case study on delta(2)H and delta(18)O of pure water samples and alcohol/water mixtures. *Rapid Commun. Mass Spectrom.* **2009**, *23*, 1879–1884. [CrossRef]
39. Gupta, S.; Jena, V.; Matic, N.; Kapralova, V.; Solanki, J. Assessment of Geo-Accumulation Index of heavy metal and source of contamination by multivariate factor analysis. *Int. J. Hazard. Mater.* **2014**, *2014*, 18–22.
40. Müller, G. Index of geo-accumulation in sediments of the Rhine River. *Geo. J.* **1969**, *2*, 108–118.
41. Turekian, K.; Wedepohl, K.H. Distribution of the Elements in Some Major Units of the Earth's Crust. *Geol. Soc. Am. Bull.* **1961**, *72*, 175. [CrossRef]
42. Bayerische Vermessungsverwaltung. Open Data: Digtales Geländemodell 1 m (DGM1). Available online: https://geodaten.bayern.de/opengeodata/OpenDataDetail.html?pn=dgm1 (accessed on 28 February 2025).
43. Wagner, B.; Töpfner, C.; Lischeid, G.; Scholz, M.; Klinger, R.; Klaas, P. Hydrogeochemische Hintergrundwerte der Grundwässer Bayerns. *GLA Fachber.* **2003**, *21*, 252.
44. Furtak, H.; Langguth, H.R. Zur hydrochemischen Kennzeichnung von Grundwässern und Grundwassertypen mittels Kennzahlen [Towards hydrochemical identification of groundwater and types of groundwater by means of indices]. *Mem IAH Cong.* **1967**, *7*, 86–96.
45. Meng, R.; Han, Z.; Gao, X.; Zhao, Y.; Han, C.; Han, Y.; Yang, R.; Li, S.; Liu, F.; Tucker, M.E.; et al. Dissolved ammonia catalyzes proto-dolomite precipitation at Earth surface temperature. *Earth Planet. Sci. Lett.* **2024**, *646*, 119012. [CrossRef]
46. Stumpp, C.; Klaus, J.; Stichler, W. Analysis of long-term stable isotopic composition in German precipitation. *J. Hydrol.* **2014**, *517*, 351–361. [CrossRef]
47. International Atomic Energy Agency. Global Network of Isotopes in Precipitation (GNIP). Available online: https://www.gtn-h.info/gtnh_networks/gnip-gnir/ (accessed on 22 February 2025).
48. Bottrell, S.; Tellam, J.; Bartlett, R.; Hughes, A. Isotopic composition of sulfate as a tracer of natural and anthropogenic influences on groundwater geochemistry in an urban sandstone aquifer, Birmingham, UK. *Appl. Geochem.* **2008**, *23*, 2382–2394. [CrossRef]
49. Burke, A.; Present, T.M.; Paris, G.; Rae, E.C.; Sandilands, B.H.; Gaillardet, J.; Peucker-Ehrenbrink, B.; Fischer, W.W.; McClelland, J.W.; Spencer, R.G.; et al. Sulfur isotopes in rivers: Insights into global weathering budgets, pyrite oxidation, and the modern sulfur cycle. *Earth Planet. Sci. Lett.* **2018**, *496*, 168–177. [CrossRef]
50. Otero, N.; Soler, A. Sulphur isotopes as tracers of the influence of potash mining in groundwater salinisation in the Llobregat Basin (NE Spain). *Water Res.* **2002**, *36*, 3989–4000. [CrossRef]
51. Relph, K.E.; Stevenson, E.I.; Turchyn, A.V.; Antler, G.; Bickle, M.J.; Baronas, J.J.; Darby, S.E.; Parsons, D.R.; Tipper, E.T. Partitioning riverine sulfate sources using oxygen and sulfur isotopes: Implications for carbon budgets of large rivers. *Earth Planet. Sci. Lett.* **2021**, *567*, 116957. [CrossRef]
52. Gammons, C.H.; Brown, A.; Poulson, S.R.; Henderson, T.H. Using stable isotopes (S, O) of sulfate to track local contamination of the Madison karst aquifer, Montana, from abandoned coal mine drainage. *Appl. Geochem.* **2013**, *31*, 228–238. [CrossRef]
53. Jiang, C.; Cheng, L.; Li, C.; Zheng, L. A hydrochemical and multi-isotopic study of groundwater sulfate origin and contribution in the coal mining area. *Ecotoxicol. Environ. Saf.* **2022**, *248*, 114286. [CrossRef] [PubMed]
54. Wang, H.; Zhang, Q. Research Advances in Identifying Sulfate Contamination Sources of Water Environment by Using Stable Isotopes. *Int. J. Environ. Res. Public Health* **2019**, *16*, 1914. [CrossRef] [PubMed]